RESEARCH ARTICLE

A Novel Continuum Robot With Stiffness Variation Capability Using Layer Jamming: Design, Modeling, and Validation

YEMAN FAN[1], **(Student Member, IEEE), DIKAI LIU**[1], **(Senior Member, IEEE), AND LIN YE**[2]
[1]Robotics Institute, Faculty of Engineering and Information Technology, University of Technology Sydney, Sydney, NSW 2007, Australia
[2]School of Aerospace, Mechanical and Mechatronic Engineering, The University of Sydney, Sydney, NSW 2006, Australia

Corresponding author: Yeman Fan (yeman.fan@student.uts.edu.au)

ABSTRACT This paper presents a novel continuum robot (*OctRobot-I*) that has controllable stiffness variation capability in both the transverse and axial directions. Robot design, stiffness variation analysis and experimental testing are discussed in detail. Stiffness models based on the Euler-Bernoulli beam theory are developed, and then four static deflection cases are analysed. Experiments are conducted with two types of layer jamming sheaths (overlap numbers $n = 3, 5$) and four different vacuum pressures (0kPa, 25kPa, 50kPa, 75kPa) at three different bending angles ($0°$, $90°$, $180°$). The results demonstrate that the stiffness changing tendency is in compliance with the derived models and show that the robot has a good stiffness variable capability. With the jamming sheath of $n = 3$, the stiffness ranges (ratios) are 36.4 to 241.7 N/m (6.6) and 92.9 to 19.3×10^3 N/m (207.8) in the transverse and axial directions, respectively. With the jamming sheath of $n = 5$, the stiffness ranges (ratios) are 65.7 to 398.3 N/m (6.1) and 106.7 to 20.8×10^3 N/m (194.9) in the transverse and axial directions, respectively. Additionally, the actuating and gripping experiments demonstrate that this robot has good performance in real-world applications.

INDEX TERMS Continuum robot, tendon-driven actuation, layer jamming, manipulator, stiffness variation.

I. INTRODUCTION

Continuum robots (CRs) are recently becoming a research focus due to their novel inherent compliance, flexibility, and dexterity [1], [2]. Because of these advantages, CRs have the potential to be applied in many application scenarios, such as medical services [3], [4], non-destructive inspections [5], and general grasping tasks [6]. However, this type of robot may suffer from many problems, and one of them is the need to improve its stiffness variation capability while keeping the same dexterity level [1], [2], [3].

Different types of stiffness tuning approaches were proposed and applied to CRs. Generally, variable stiffness capability in CRs can be achieved by utilising antagonism mechanisms, phase transition materials, external magnetic fields, and jamming mechanisms [7], [8], [9]. Antagonism

The associate editor coordinating the review of this manuscript and approving it for publication was Zheng Chen.

mechanisms realise stiffness variation based on a pair of antagonistic forces, which can be easily achieved in tendon-driven or artificial-muscle CRs [10], [11]. Although antagonism mechanisms are simple and easy to implement, their efficiency is relatively low and it needs great extra force or high muscle pressure to form antagonistic force pairs, which would result in heavy mass in actuators, i.e. large driven motor or air pump.

Phase transition materials can be part of or filled into the body of CRs to achieve stiffness variation. In [12], a CR for MRI-Guided neurosurgery was presented, the robot backbone was made of shape memory alloy (SMA) springs, and the stiffness control was achieved by directly powering the SMA spring to increase its temperature. There was no active cooling system in this robot, which means it would take a long time to change to rigid status. In order to improve the stiff switching time, researchers applied cold and hot water into the temperature control system. In [13], a special

structure was designed to achieve fast stiffness variation (in 15 seconds) of the continuum manipulator made by low melting point alloy (LMPA) material. In [14], a LMPA-made manipulator was designed for minimally invasive surgery (MIS) with actively rigid and flexible states controlling (state switch time of 9.2-10.3s and 15.4s). Similarly, a flexible endoscope manipulator using shape memory polymer (SMP) was proposed in [15]. Although phase transition materials can achieve variable stiffness, they have the disadvantage of either long response time (passive cooling) or large-size and heavy-mass temperature management systems (water cycling).

Another stiffness variation method is to use electrorheological (ER) or magnetorheological (MR) fluids. When applying an external magnetic field, their stiffness can be achieved by changing their viscosity. A manipulator based on MR compounds for laparoscopic surgery was presented in [16]. However, MR/ER fluids need a strong magnetic field to change their viscosity and often have limitations in achieving sufficiently high stiffness or yield strength.

Among the stiffness variable technologies, jamming mechanisms are promising when applied to CRs due to their advantages of easy realisation, shape-locking capability, and quick activation. Generally, jamming technology can be divided into fibre jamming, particle jamming, and layer jamming according to its filling materials [7], [8]. In fibre jamming and particle jamming mechanisms, the jamming materials are normally filled into CRs and work as main bodies [17], [18], [19]. Compared to particle jamming and fibre jamming, layer jamming uses thin plastic or paper layers as its jamming flaps and can be easily applied to CRs as a reinforcing sheath [20], [21], which results in the advantages of lighter weights and taking up less space of CRs.

In [22], layer jamming flaps were wrapped into a cylinder shape to form a manipulator for MIS. A two-section prototype robot based on spring and layer jamming was designed in [23]. In [24], a flexible variable stiffness robot combined with layer jamming and backbone was developed for nephrectomy. However, these works are limited to small diameters and stiffness reinforcement ability [8]. Additionally, their actuator units were not compact and took large space than the robot body. In order to increase stiffness reinforcing ability, several robots with larger diameters were designed. In [19], six different continuum manipulator structures (diameters of 41∼48mm) utilising both granular and layer jamming mechanisms were implemented. In [25] and [26], a malleable robot combining layer jamming with a flexible spine was developed. In [27], a stiffness-tuneable segment for continuum soft robots with vertebrae was presented. A revolute joint based on layer jamming for robotic exoskeletons was developed [28]. In [29], stiffening sheaths based on layer jamming were built for continuum robots. These robots have improved with larger diameters, however, they were limited to shorter lengths, and there were no actuators.

In the above CRs, layer jamming was sewn along the guide holes and slots by an extra thread to form sheaths. Once the

layer pattern was set, the sheaths' length-changing ability was mainly determined by the slot length, which was small (4mm in [25]) and may affect the length change range. In addition, the design and test targets of previous research were focused on robots' performance in the transverse direction, and there was no testing conducted in the axial direction [19], [22], [24], [25], [26].

Furthermore, although some analytical models were researched for CRs under external loads, these models focused on the effect of the tendon's number or displacement, and they were based on the cantilever beam model [30] or Euler-Lagrange equations [31]. To the best of the authors' knowledge, research works related to approximate models of continuum robots' effective stiffness are seldom conducted.

In this paper, we present a novel continuum robot called *OctRobot-I*. Layer jamming sheaths and a support spine are designed to achieve stiffness variation capability in both the transverse and axial directions. In order to evaluate the robot's performance, extensive force-deflection experiments are conducted in both two directions, and actuating and gripping capabilities are validated and demonstrated. The main contributions of this work include:
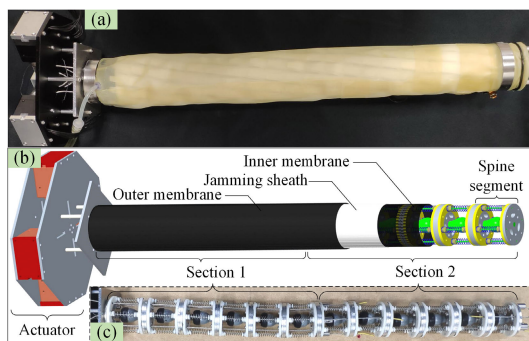
i) A new layer jamming sheath weaving method is proposed for continuum robots. Compared to the previous research, this method uses restriction wires on the adjacent two layers to restrict the flap and provide a larger relative movement ability.

ii) Approximate stiffness models are developed and used for analysing the robot's effective stiffness and its changing tendency.

iii) A novel continuum robot with stiffness variation capability in both the transverse and axial directions is designed and fabricated.

iv) Experimental verifications of the continuum robot are conducted to test its stiffness variation performance.

The rest of this paper is organised as follows. Section II presents the design scheme of the robot. Section III describes the approximate stiffness models of the robot. Section IV presents the testing experiments and stiffness results. Discussions are presented in Section V, and a conclusion is addressed in Section VI.

II. ROBOT DESIGN
A. OVERALL DESIGN OF THE CONTINUUM ROBOT
In nature, many organs have a continuum structure, such as elephant trunks, tentacles, and tongues. These organs are very flexible and also have excellent load capacity. One good example that inspired many researchers is the octopus tentacle [1]. Although octopus tentacles lack rigid structures, it has unique biomechanical capabilities that combine significant flexibility with the ability to change and control their stiffness. Therefore, by imitating an octopus tentacle's structure and motion mechanism, a novel continuum robot named *OctRobot-I* is designed and implemented, as shown in Fig. 1.

Y. Fan et al.: Novel Continuum Robot With Stiffness Variation Capability Using Layer Jamming: Design, Modeling, and Validation

IEEE Access

FIGURE 1. The developed novel continuum robot. (a) Photo of the continuum robot. (b) A sectional view of the CAD model showing components and overall length/width ratio. (c) Photo of the support spine of the robot.

TABLE 1. Physical properties and performance of the continuum robot.

| Properties	Value
Total robot length	572 mm
Actuator	68 mm
Robot body	504 mm
Total robot weight	1.7 kg
Actuator	0.8 kg
Robot body	0.9 kg
Robot outer diameter	~50 mm
The number of spine segments	12 (6/section)
Degrees of freedom	4 (2/section)
Maximum bending degree	180°

The continuum robot consists of a support spine, inner membrane, jamming sheath, outer membrane, and actuator unit. The support spine uses ball joints to offer axial support capability, and the jamming sheath is used to realise stiffness variation capabilities in both the transverse and axial directions when compressed. To compress the jamming sheath and activate its stiffening mechanism, two tubular latex membranes (thickness of 0.3mm) are selected to seal the whole jamming sheath when evacuating the tubular volume between the two membranes [19], [22], [25]. The whole robot consists of two sections. Each section is controlled by two pairs of cables, which provide the robot with four degrees of freedom in total. The continuum robot properties are summarized in Table 1.

B. SUPPORT SPINE AND ACTUATOR
1) SPINE SEGMENT
The whole support spine is made of 12 connected spine segments, as shown in Fig. 1(c). A single segment is composed of two custom aluminium disc spacers, one pair of spring constraint discs, four helical compression springs, a ball joint (SQZ5-RS, China), and a grub screw, as shown in Fig. 2.

In order to ensure that the spine segment can provide support in the axial direction, the ball joint (maximum tilt
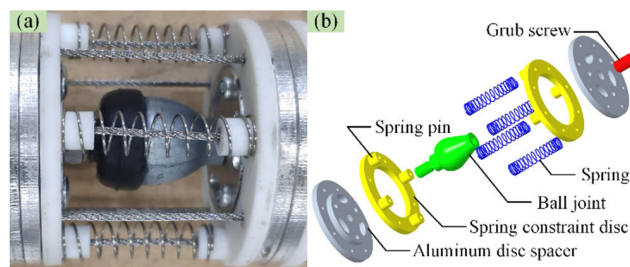
FIGURE 2. A support spine segment. (a) Overall assembly photo. (b) Exploded-view drawing.

angle of 30°) is used in each segment to make sure it has both the flexible bending ability and the hard contact ability. Since ball joints lack self-recovery ability, four helical compression springs (measured spring constant 493N/m) are mounted around the ball joint to provide a certain force for the spine to recover to its original position. In addition, the aluminium disc spacer and spring constraint disc are used as support for the outside layer jamming. The spring constraint disc is 3D printed using polylactic acid (PLA) materials, and it has four small pins arranged at 90° to mount and constrain the springs. In order to connect the adjacent segments, three aluminium rivets (Φ3.2 × 12mm) are used and arranged at 120° intervals.
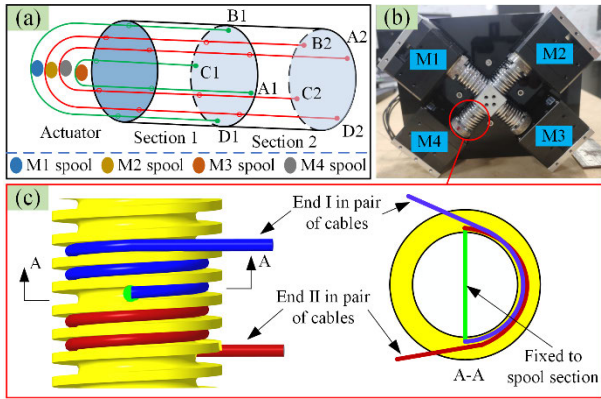
2) ACTUATOR UNIT
In order to actuate the cables for controlling the robot, an actuator unit is designed by using servo motors and tailored aluminium spools. Unlike the robot actuated by ball screws [22] and worm gears [24], this design offers a compact, lightweight, low-volume actuator unit. Fig. 3(a) shows the concept of four pairs of cables to actuate the whole continuum robot. The robot has two sections with each section driven by two pairs of cables. Stainless steel wire rope with a diameter of 1.2mm is selected. The rope is mounted in the spools, and its two ends go through its controlling section arranged at an interval of 180°. All the rope ends are fixed on the surface of the last aluminium disc spacer in each section.

Fig. 3(b) and (c) show the design of the actuator unit and the spool mechanism employed in this continuum robot. The actuator unit is composed of four servo motors (XM430-W350, DYNAMIXEL), four tailored aluminium spools, four pairs of stainless-steel wire ropes, and support frames. In the spool mechanism, the cable goes through the lateral hole of the spool. The two ends of the cable are helically coiled on the spool in the clockwise and counterclockwise directions, respectively. Thus, the same cable length can be fed in and pulled out from both sides (End I and End II) by the rotation of the motor, which can maintain the cable tension at any configuration.

C. JAMMING SHEATH
1) JAMMING FLAP STRUCTURE
The structure of the jamming layer for this continuum robot is based on the double-side flap pattern described in [22].

IEEE *Access*

Y. Fan et al.: Novel Continuum Robot With Stiffness Variation Capability Using Layer Jamming: Design, Modeling, and Validation

FIGURE 3. (a) Diagram of the driving cable arrangement of the robot, A1-D1 are for controlling Section 1 (green), A2-D2 are for controlling Section 2 (red). (b) Picture of the actuator unit. Note that the motors labelled M1/M3 and M2/M4 were spaced 90° apart for controlling Section 1 and Section 2, respectively. (c) Diagram of a spool mechanism.
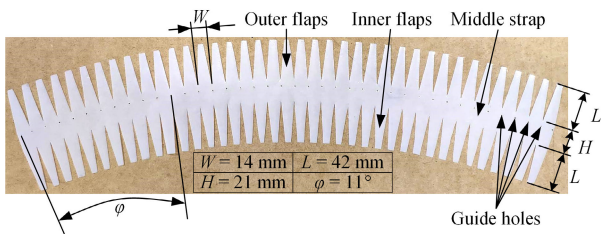

FIGURE 4. Layer jamming in the double-side flap pattern with guide holes.

In order to suit our support spine of larger diameter (45mm), the flap width W, middle strap length H, flap length L, and inclination angle φ are selected according to the requirements in this research, as shown in Fig. 4.

In order to make this double-side flap, the polyvinyl chloride (PVC) window film (Wf1224pf, Pillar, Australia) with a thickness of 0.18mm is used and cut into the double-sided shape. The front and back sides of this film have different surface roughness, with each side contacting the opposite side when weaving into a sheath. The measured coefficient of friction (COF) is 0.5 between the two sides.

2) JAMMING SHEATH WEAVING METHOD

When the continuum robot is bending, the layer jamming sheath is required to change its length correspondingly because the convex position will become longer while the concave position will be shorter. Therefore, the layer jamming sheath should have enough length changing ability to ensure that the continuum robot can bend at enough angle to meet task requirements. For making the layer jamming sheath, researchers [22], [25], [26], [27], [29] used the guide hole and slot method. In that method, jamming flaps were restricted by a line going through the holes and slots, and the restriction line could shift in the slot. This provided the adjacent overlapping jamming flaps to move relative to each other, resulting in a length change of the whole sheath.
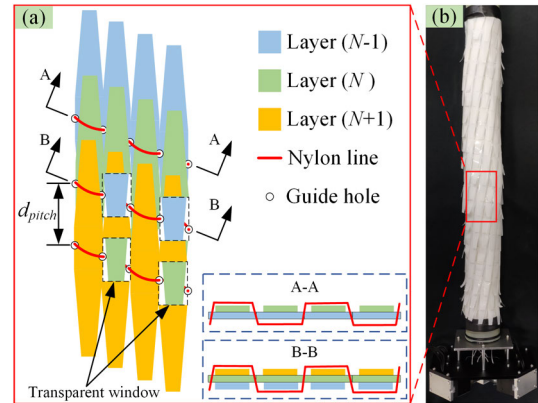
FIGURE 5. (a) Diagram of the weaving method. (b) Assembled layer jamming sheath that covers the support spine.

However, that method had a limitation regarding the length changing ability of the layer jamming sheaths due to the slot being too short (4mm in [25]).

In order to improve the length changing ability of the layer jamming sheath, a new weaving method is proposed to wind up the layer jamming into a tube sheath. To explain the weaving method, arbitrary adjacent three layers are selected. As shown in Fig. 5(a), a nylon wire with a diameter of 0.6mm goes through the external side and internal side of all the jamming flaps alternately via the guide holes. The nylon line between the two guide holes is utilised for restricting the jamming flaps. The outer flaps and inner flaps of Layer (N) are inserted into the restriction nylon line on Layer ($N-1$) and Layer ($N+1$), respectively. Therefore, the outer flaps of the Layer (N) are confined by the line on the Layer ($N-1$), whereas the inner flaps of the Layer (N) are astricted by the line on the Layer ($N+1$). The two sectional view figures (A-A and B-B in Fig. 5(a)) show the insert position and restriction approach for the flaps. By this approach, the adjacent layers can be woven into a tube sheath and still have the capability to be bent, shrunk, and elongated arbitrarily. The completed layer jamming sheath is shown in Fig. 5(b).

D. JAMMING SHEATH LENGTH CHANGE EVALUATION

The stiffness reinforcement capability of a jamming sheath is determined by the force F required to detach the contact layers. According to the research in [22] and [28], this force can be calculated as $F = \mu n PS$, where μ is the COF of the flaps, n is the layer overlap number, P is the applied pressure, and S is the overlap area which is determined by the overlap width and length of the flap. From this equation, two variables can be adjusted to vary stiffness once the flap pattern is set. The first one is P, which means different applied pressures would change the compression level of the jamming flaps. Then the cumulated friction results in a significant increase in rigidity. The second variable, different layer overlap numbers (n), can be used when winding up the layer jamming sheath to change its thickness.

Y. Fan et al.: Novel Continuum Robot With Stiffness Variation Capability Using Layer Jamming: Design, Modeling, and Validation

IEEE *Access*

According to this jamming flap structure, different layer overlap numbers (n) can be achieved by applying different winding pitches (d_{pitch}) as

$$n = (2L + H)/d_{pitch} \quad (1)$$

This is to ensure the inner and outer flaps are always moving relatively within the restriction nylon line and never out of the restriction. While ignoring the distortion of the flaps when weaving into a tube shape, the winding pitch range of this double-side flap is determined by

$$H/2 < d_{pitch} < L + H/2 \quad (2)$$

Because the layer jamming sheath is used to cover the support spine, its default length should be the same length as the support spine (l). When the robot is bending, adjacent jamming flaps will generate relative movement and then result in corresponding length changes of jamming sheaths as calculated by

$$\begin{cases} \Delta l = \beta(l/\beta \pm 25) - l = \pm 25\beta \\ d_r = \Delta l/(l/d_{pitch}) \end{cases} \quad (3)$$

where Δl is the length change of jamming sheaths and the plus and minus are the representation of the elongation (convex position) and contraction (concave position) of the jamming sheaths, respectively; β is the central angle of the robot when bending; d_r is the relative movement distance of adjacent jamming flaps.

In order to evaluate the designed jamming sheaths, the minimum and maximum length changes of jamming sheaths are calculated by

$$\begin{cases} \Delta l_{\min} = l(H/2)/d_{pitch} - l \\ \Delta l_{\max} = l(L + H/2)/d_{pitch} - l \end{cases} \quad (4)$$

In this research, $d_{pitch} = 35$mm and 21mm are selected when weaving the layer jamming sheath on the support spine. Hence, the overlap layer numbers $n = 3$, and 5, respectively. Then the minimum and maximum length changes of jamming sheaths are $\Delta l_{\min} = -352.8$mm ($n = 3$), $\Delta l_{\max} = 252.0$mm ($n = 3$), $\Delta l_{\min} = -252.0$mm ($n = 5$), and $\Delta l_{\max} = 756.0$mm ($n = 5$), respectively. From these results, it can be seen that both two types of jamming sheaths can meet the length change requirements of $\Delta l = \pm 78.5$mm when the robot is at the maximum designed bending angle of 180° with an outer diameter of 50mm. The relative movement distance of adjacent jamming layer flaps are $d_r = \pm 5.5$mm ($n = 3$) and $d_r = \pm 3.3$mm ($n = 5$), respectively.

III. APPROXIMATE STIFFNESS MODELS
A. MODEL DESCRIPTION

For analysing the stiffness and its changing tendency for the continuum robot under different conditions, corresponding stiffness models are needed. However, due to the complex structure and stiffness variability of the robot, it is hard to develop ideal beam models, and even finite element analysis
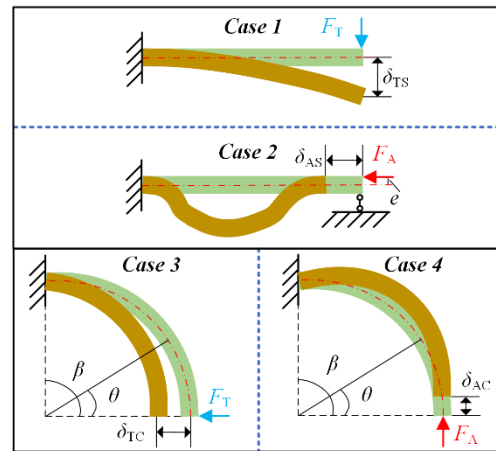

FIGURE 6. Four study cases for the equivalent beam. Case 1 Straight beam under transverse load, Case 2 Straight beam under axial load, Case 3 Curved beam under transverse load, Case 4 Curved beam under axial load.

has limitations because several parameters of the robot, including mechanical error, friction, and the jamming mechanism, are difficult to model in simulation software. In order to define and qualitatively analyse the robot's effective stiffness and its changing tendency, approximate stiffness models are trying to be developed based on the Euler-Bernoulli beam theory [32]. To represent the continuum robot with an equivalent beam model, three assumptions are made [31], [33] as follow:

1) The deflection of the continuum robot is only caused by the position change of all movable parts of the robot, and material strain is not considered.

2) The analysis of continuum robot deflection is conducted in the horizontal plane, and gravity is not considered.

3) The deflection of the continuum robot under external load has the same feature as a beam.

Based on the above assumptions, the continuum robot is now modelled as an equivalent cylindrical beam because it consists of two main cylindrical parts: a support spine and a jamming sheath (SI: Equivalent Beam).

According to different shapes and load conditions of the continuum robot, deflections of the equivalent beam can be generally categorised into four cases, as shown in Fig. 6. When the robot is straight, its deflections can be analysed based on the cantilever beam model or fixed-fixed beam model depending on the directions of external loads [32]. When the robot is bent, its deflections can be analysed based on a cantilever beam model. In order to derive equations for analysing the effective stiffness and its changing tendency, the following assumptions are made for the equivalent beam [32], [34]:

1) The equivalent beam is homogeneous and obeys Hooke's law.

2) Displacements of the equivalent beam are small.

3) The equivalent beam is in pure bending when it has deflections. (SI: Euler-Bernoulli Beam)

B. MODEL DERIVATION

In this section, the robot's effective stiffnesses in the four cases are analysed and derived corresponding to the four deflection cases. *Case 1*, *3* and *4* are solved based on the Maxwell-Mohr method [21], while *Case 2* is based on the integral method [32].

In the Maxwell-Mohr method, the deflection of a beam can be calculated as

$$\delta(x) = \int \frac{M(x)\overline{M}(x)}{D} dx \qquad (5)$$

where $\delta(x)$ is the deflection at x position, $x \in [0, l]$ is the analytical position on the beam, $M(x)$ is the resultant moment at x by an external load, $\overline{M}(x)$ is the moment at x due to the unit load, D is flexural rigidity of the beam. (SI: Maxwell-Mohr Method)

1) CASE 1 STRAIGHT BEAM UNDER TRANSVERSE LOAD

When the continuum robot is straight, and the transverse load F_T is applied at the tip position, the resultant moment and unit moment at section x are

$$\begin{cases} M(x) = F_T x \\ \overline{M}(x) = x \end{cases} \qquad (6)$$

By substituting (6) into (5) and letting $x = l$, the effective stiffness in this case can be defined as

$$k_{TS} = F_T/\delta_{TS} = F_T/\delta(x)\,|_{x=l} = 3D/l^3 \qquad (7)$$

where $\delta_{TS} = \delta(x)\,|_{x=l}$ is the deflection at the tip position.

2) CASE 2 STRAIGHT BEAM UNDER AXIAL LOAD

When the continuum robot is straight, and the external load F_A is applied on the robot's central axis, the stiffness of the robot in the axial direction should be infinite when ignoring the material strain. However, due to mechanical errors and assembly errors, the central lines of all movable parts cannot be kept in an exact line with the robot's central axis. Hence, infinite stiffness is only a theoretical stiffness under ideal conditions. In order to analyse the effective stiffness in the axial direction, we assume that there is a distance error (e) between the external load direction and the robot's central axis. In addition, an extra lateral force will be generated to restrict the robot's lateral motion when the axial load is applied to the robot. Hence, the robot deflection can be analysed based on the fixed-fixed model [32], and its governing equation and general solution are

$$\begin{cases} \dfrac{d^4\delta(x)}{dx^4} + a^2\dfrac{d^2\delta(x)}{dx^2} = 0, \quad a^2 = \dfrac{F_A}{D} \\ \delta(x) = C_1\cos ax + C_2\sin ax + C_3 x + C_4 \end{cases} \qquad (8)$$

where C_1, C_2, C_3, C_4 are constants.

According to the Euler-Bernoulli beam theory, the boundary conditions for the fixed-fixed model are

$$\begin{cases} \delta(x)\,|_{x=0} = 0, \quad \delta(x)\,|_{x=l} = 0 \\ \delta''(x)\,|_{x=0} = 0, \quad \delta''(x)\,|_{x=l} = -F_A e/D \end{cases} \qquad (9)$$

Substituting boundary conditions (9) into (8), the explicit deflection solution is

$$\delta(x) = e(\sin ax/\sin al - x/l) \qquad (10)$$

In (10), since $\sin al$ appears in the denominator, the deflection $\delta(x)$ will become infinite when $al = b\pi, (b \in Z)$. This phenomenon is called buckling, and the corresponding axial load is

$$F_A = b^2\pi^2 D/l^2 \qquad (11)$$

When $b = 1$, $F_{cr} = F_A\,|_{b=1} = \pi^2 D/l^2$ is the critical load of bulking. Once the external load $F_A \geq F_{cr}$, the beam will buckle, and its stiffness will dramatically decrease. Since the tip deflection δ_{AS} is caused by the deflection $\delta(x)$ and both the two deflections are small, we assume $\delta_{AS} = \max[\delta(x)]$, then the effective stiffness in this case is

$$k_{AS} = F_T/\delta_{AS} = F_A/\max[\delta(x)], \quad F_A < F_{cr} \qquad (12)$$

3) CASE 3 CURVED BEAM UNDER TRANSVERSE LOAD

When the continuum robot is curved at a central angle $\beta \in (0, \pi]$, and the transverse load F_T is applied at the tip position, the resultant moment and unit moment at x position are

$$\begin{cases} M(\theta) = F_T l \sin\theta/\beta \\ \overline{M}(\theta) = l\sin\theta/\beta \end{cases} \qquad (13)$$

where $\theta = \beta(l-x)/l$ is the central angle between x position and the tip position.

By substituting (13) into (5) and letting $x = l$, after correspondingly conversing coordinates, the effective stiffness in this case is defined as

$$\begin{aligned} k_{TC} &= F_T/\delta_{TC} = F_T/\delta(\theta)\,|_{x=l} \\ &= 4D\beta^3/l^3(2\beta - \sin 2\beta) \end{aligned} \qquad (14)$$

where $\delta_{TC} = \delta(\theta)\,|_{x=l}$ is the deflection at the tip position.

Noted that $\beta^3/(2\beta - \sin 2\beta)$ in (14) is monotonically increasing about β. Hence, the effective stiffness k_{TC} will increase when increasing the robot's central angle β.
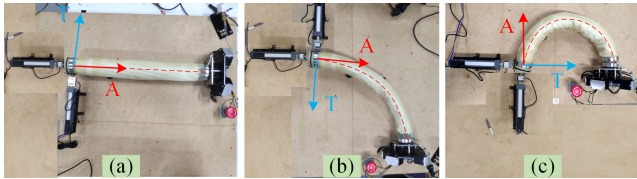
4) CASE 4 CURVED BEAM UNDER AXIAL LOAD

This case is the same as *Case 3* while the external load F_A is in the axial direction. When the axial load F_A is applied at the tip position, the resultant moment and unit moment at x position are

$$\begin{cases} M(\theta) = F_A l(1 - \cos\theta)/\beta \\ \overline{M}(\theta) = l(1 - \cos\theta)/\beta \end{cases} \qquad (15)$$

By substituting (15) in (5) and letting $x = l$, after correspondingly conversing coordinates, the effective stiffness in this case is defined as

$$\begin{aligned} k_{AC} &= F_A/\delta_{AC} = F_A/\delta(\theta)\,|_{x=l} \\ &= 4D\beta^3/l^3(6\beta - 8\sin\beta + \sin 2\beta) \end{aligned} \qquad (16)$$

where $\delta_{AC} = \delta(\theta)\,|_{x=l}$ is the deflection at the tip position.

Y. Fan et al.: Novel Continuum Robot With Stiffness Variation Capability Using Layer Jamming: Design, Modeling, and Validation

IEEE *Access*

FIGURE 7. Experiment setup. (a) Robot at 0° bending. (b) Robot at 90° bending. (c) Robot at 180° bending. Note that A and T in the figure represent the axial and transverse directions, respectively.

Noted that $\beta^3/(6\beta - 8\sin\beta + \sin 2\beta)$ in (16) is mainly monotonically decreasing about β. Hence, the effective stiffness k_{AC} will decrease when increasing the robot's central angle β.

When the robot is in a straight shape, equation (7) shows that the effective stiffness k_{TS} is a constant with a specific flexural rigidity (D); equation (12) shows that the effective stiffness k_{AS} is divided into two levels by the critical load (F_{cr}): high stiffness before buckling and low stiffness after bucking. When the robot is bent, considering the monotonicity of equations (14) and (16), two specific curved angles ($\beta = 90°, 180°$) in the middle point and end point of the angle range ($\beta \in (0, \pi]$) are selected for the stiffness experiments because the effective stiffness k_{TC} and k_{AC} about the curved angle (β) are increasing and decreasing, respectively.

IV. EXPERIMENTS AND RESULTS
A. EXPERIMENT SETUP
A test rig is built for experiments to test the robot's stiffness under different loading conditions. It consists of a linear actuator (L12-210-100-12I, Actuonix) and an S-Beam load cell (JLBS-M2-10Kg) to generate target deflections and collect resistance forces, respectively. In addition, a vacuum pump (KMDP-C1-12V) and a pressure sensor (DP-101A-E-P, Panasonic) are used to generate different vacuum pressures. To investigate the stiffness variation capability, the robot is tested at three different bending angles (0°, 90°, 180°) and four different vacuum pressures (0kPa, 25kPa, 50kPa, 75kPa). The tests are shown in Fig. 7. In these experiments, the external load at the transverse and axial directions are applied separately.

B. FORCE-DEFLECTION RESULTS
All the experimental data was collected and analysed using MATLAB software. Each experiment was repeatedly conducted five times under the same condition, and the mean value of the measured force in an experiment was calculated. Error bars shown in the plots are ±1 standard deviation for every 5mm deflection (transverse direction) and every 2mm deflection (axial direction). The force-deflection results of the continuum robot are shown in Fig. 8 and Fig. 9.

From Fig. 8, it can be seen that both two types of jamming sheaths can enforce the resistance force in both the transverse and axial directions when vacuum pressures are applied, and the jamming sheath ($n = 5$) shows better ability than the
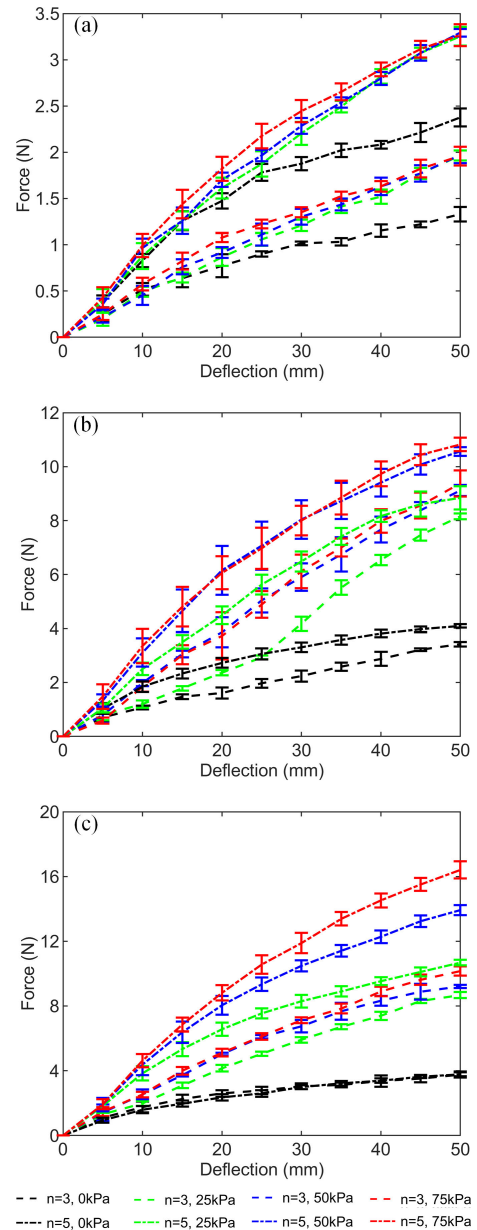
FIGURE 8. Force-deflection plots of the robot under transverse (T direction) loads: (a) At 0° bending. (b) At 90° bending. (c) At 180° bending.

jamming sheath ($n = 3$). When the bending angle is 0° (Fig. 8(a)), because all jamming layers are tightly contacted, and there is no relative slip when vacuum pressure is applied, it shows the same stiffness tuning ability under different pressures [21]. Hence, the resisting forces are almost the same under the three vacuum pressures (25kPa, 50kPa, 75kPa), with the maximum values of 2.0N ($n = 3$) and 3.3N ($n = 5$). When the bending angle is 90° (Fig. 8(b)), the overlap area of contacted jamming layers is changed, and it needs higher vacuum pressure to maintain no relative slip. Hence, the resisting force data of 50kPa and 75kPa are almost overlapping and higher than 25kPa (slip occurred). The maximum resisting
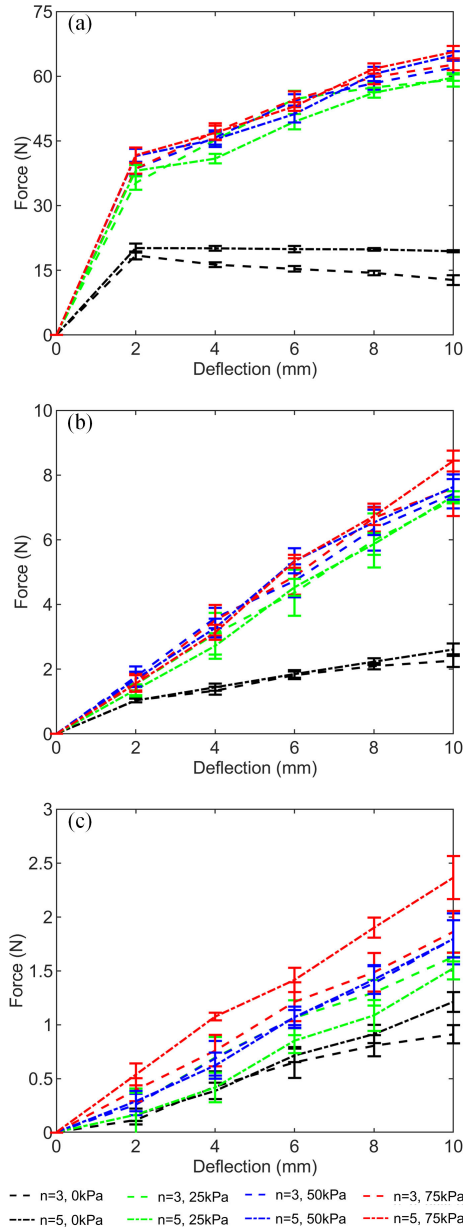
IEEE *Access*

Y. Fan et al.: Novel Continuum Robot With Stiffness Variation Capability Using Layer Jamming: Design, Modeling, and Validation

FIGURE 9. Force-deflection plots of the robot under axial (A direction) loads: (a) At 0° bending. (b) At 90° bending. c) At 180° bending.

forces are 9.4N (n = 3, 75kPa) and 10.8N (n = 5, 75kPa). When the robot is bent by 180° (Fig. 8(c)), in the convex part, the jamming layer overlap area becomes much less, and it would be easier for the relative slip to occur. After deflection of 15mm, both two types of jamming sheaths show contact layers slipping under all the vacuum pressures and resulting in different resisting forces. The maximum resisting forces in this situation are 10.2 N (n = 3, 75kPa) and 16.4N (n = 5, 75kPa).

In the axial direction, Fig. 9(a) and (b) show that the three different vacuum pressures (25kPa, 50kPa, 75kPa) have a negligible effect on changing the resisting force. This is because the axial loads can hardly detach the contact jamming layers, and jamming sheaths always keep at the

no-slip condition at all vacuum pressures. Therefore, higher vacuum pressure will not result in a better stiffening effect due to no relative slip occurring. When the bending angle is 0° (Fig. 9(a)), the resistance forces are at the highest level and greater than in any other situation because ball joints on the support spine can provide hard contact in the axial direction, and jamming sheaths cover the spine to restrict its tilt movement. The maximum resisting force is 62.6N (n = 3) and 65.6N (n = 5) under the vacuum pressure of 75kPa. When the bending angle is 90° (Fig. 9(b)), the robot shows almost the same resisting force under the vacuum pressure of 25kPa, 50kPa and 75kPa, with a maximum value of 7.6N (n = 3, 75kPa) and 8.4N (n = 5, 75kPa). When the bending angle changes to 180° (Fig. 9(c)), the contact layers are more likely to slip due to the change in the overlap area. Therefore, the resisting forces are different under all the vacuum pressures, and at the lowest level with the maximum values of 1.9N (n = 3, 75kPa) and 2.4N (n = 5, 75kPa).

C. STIFFNESS VARIATION RESULTS
In order to reduce errors and compare the stiffness under different conditions, average stiffness is calculated based on the force-deflection data presented in Fig. 8 and Fig. 9.

1) STIFFNESS IN THE TRANSVERSE DIRECTION
According to equations (7) and (14), the effective stiffness k_{TS} and k_{TC} should be constant with a specific flexural rigidity (D). However, the experimental data in Fig. 8(a)-(c) are only approximately linear. This error may result from the friction disturbance in the test rig, or the robot may not be perfectly replaced by an equivalent beam model when it has deflections because of complex structures and mechanical errors of the robot. Therefore, to eliminate errors, the average stiffness of the robot is calculated by

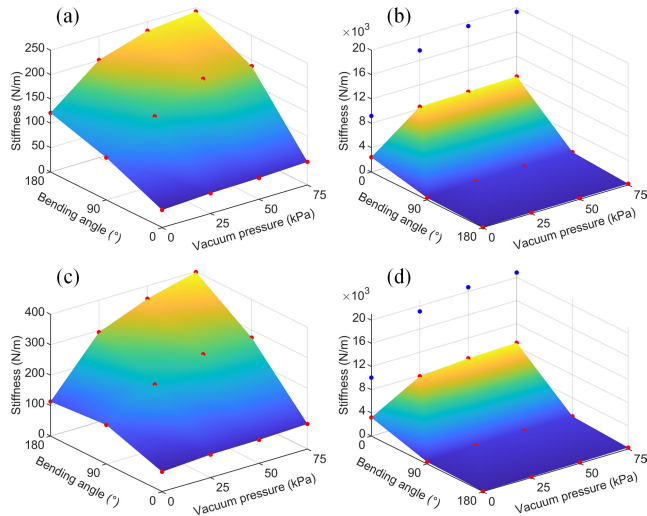$$S_{\mathrm{T}} = \sum_{i=1}^{10} \frac{F_i}{\delta_i}/10 \qquad (17)$$

where S_{T} is the average transverse stiffness, F_i is the resisting force at point i, δ_i is the deflection at point i, i is the deflection point at Fig. 8(a)-(c), starting at 5mm and increasing 5mm each time to 50mm.

2) STIFFNESS IN THE AXIAL DIRECTION
When the robot is straight, as analysed in *Case 2*, the effective stiffness keeps at a high level before critical load and will decrease to a low level once the robot buckles. In Fig. 9(a), this phenomenon can be clearly seen. Before the 2mm deflection, the robot shows high stiffness and then decreases to a low level with the deflection increasing, especially in no vacuum pressure conditions. Therefore, the robot stiffness should be divided into two parts and calculated as

$$S_{\mathrm{AS}} = \begin{cases} F_{j=1}/\delta_{j=1}, \ (F_j < F_{\mathrm{cr}}) \\ \sum_{j=2}^{5} \frac{F_j}{\delta_j}/4, \ (F_j \geq F_{\mathrm{cr}}) \end{cases} \qquad (18)$$

Y. Fan et al.: Novel Continuum Robot With Stiffness Variation Capability Using Layer Jamming: Design, Modeling, and Validation

IEEE *Access*

FIGURE 10. Average stiffness results. (a) Transverse direction with n = 3. (b) Axial direction with n = 3. (c) Transverse direction with n = 5. (d) Axial direction with n = 5. Note that the red dots denote the average stiffness, and the blue dots denote the stiffness before buckling.

FIGURE 11. Photos of the robot actuating and gripping experiments. (a)-(f) The robot is at different bending postures. (g) The robot is gripping a paper roll with a weight of 590g and a diameter of 145mm. (h) The robot is gripping an iron bucket with a weight of 1.2kg and a diameter of 180mm. (i)-(l) The robot is moving a piece of iron (511g) using its end-effector, (i)-(j) show a normal moving task, and (k)-(l) show the task with the obstacle. (Supplementary Videos).
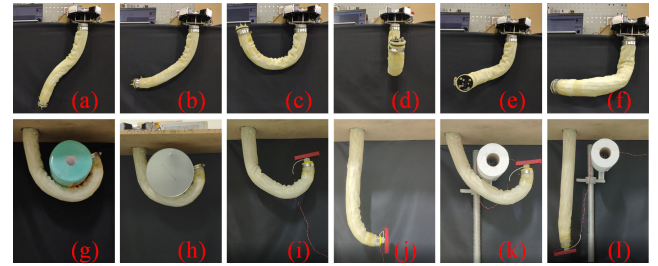
where S_{AS} is the average axial stiffness when the robot is straight, F_j is the resisting force at point j, δ_j is the deflection at point j, j is the deflection point at Fig. 9(a), starting at 2mm and increasing 2mm each time to 10mm.

When the robot is bent, equation (16) shows that the effective stiffness k_{AC} is constant at a specific bending angle, and the experimental data in Fig. 9(b) and (c) also show a linear relationship between force and deflection. Hence, the average stiffness is calculated as

$$S_{AC} = \sum_{j=1}^{5} \frac{F_j}{\delta_j}/5 \qquad (19)$$

As shown in Fig. 10, the average stiffness results show that the vacuum pressure can change the robot stiffness at any condition, and the jamming sheath with a layer overlap number $n = 5$ has greater stiffness increasing ability compared to $n = 3$. The robot stiffness increases and decreases with the bending angle increasing in the transverse direction and axial direction, respectively. In the transverse direction, the robot is bent 0° with a vacuum pressure of 0kPa has the minimum stiffness, i.e. 36.4N/m ($n = 3$) and 65.7N/m ($n = 5$), whereas the robot at the bending angle of 180° with a vacuum pressure of 75kPa has the maximum stiffness of 241.7N/m ($n = 3$) and 398.3N/m ($n = 5$). At the bending angle of 90°, the stiffness is between that at bending 0° and 180° under each vacuum pressure.

In the axial direction, when the robot is straight and not buckling, the robot stiffness increases from 9.2×10^3 N/m to 19.3×10^3 N/m ($n = 3$) and 10.1×10^3 N/m to 20.8×10^3 N/m ($n = 5$) when the vacuum pressure changes from 0kPa to 75kPa. As presented before, this high stiffness is mainly a result of the mechanical stiffness of the support spine. After buckling, the maximum average stiffness decreases to 8.6×10^3 N/m ($n = 3$, 75kPa) and 8.7×10^3 N/m

($n = 5$, 75kPa). When the robot is at a bending of 180°, it has a minimum stiffness of 92.9N/m ($n = 3$) and 106.7N/m ($n = 5$) at the vacuum pressure of 0kPa, and the stiffness increases to 192.4N/m ($n = 3$) and 249.7N/m ($n = 5$) when the vacuum pressure reached 75kPa. Similarly, the stiffness has the same changing trend when the bending angle is 90°, from 328.6N/m ($n = 3$, 0kPa) and 344.5N/m ($n = 5$, 0kPa) rising to 816.6N/m ($n = 3$, 75kPa) and 827.1N/m ($n = 5$, 75kPa), respectively.

D. ACTUATING AND GRIPPING EXPERIMENTS

The designed prototype robot can be deployed as a general manipulator for completing tasks including gripping, moving, and inspection. Due to its inherent compliance and flexibility, this prototype robot can carry an object by its body or end-effector, and it can easily reach behind obstacles. Experiments about actuating and gripping are conducted to demonstrate that this robot performs well. As an example, an electromagnet (GE-66-100-38, Magnetic Sensor Systems, USA) is attached to the distal of the robot and works as an end-effector in moving tasks. The robot performance demonstrations are shown in Fig. 11.

V. DISCUSSION

The designed continuum robot uses ball joints to offer axial support, and stiffness variation capabilities in both the transverse and axial directions are realized by combining with the jamming sheaths. Compared to previous research, this design has the advantages of higher axial stiffness, larger length changing ability of jamming sheaths, and a compact actuator unit. Therefore, this robot can be deployed to different applications and work as a manipulator or end-effector.

In the four stiffness cases, although the effective stiffness k_{TS}, k_{TC}, k_{AS}, and k_{AC} of the continuum robot cannot be numerically calculated due to the flexural rigidity (D) being hard to obtain because of the complex structure and stiffness variability of the robot, the stiffness changing tendency in the four cases can instead be analysed qualitatively. When the robot is straight, the effective stiffness k_{TS} is a constant with a specific flexural rigidity (D), and the effective stiffness

IEEE *Access*

Y. Fan et al.: Novel Continuum Robot With Stiffness Variation Capability Using Layer Jamming: Design, Modeling, and Validation

k_{AS} is divided into two levels by the critical load (F_{cr}): high stiffness before buckling and low stiffness after bucking, and the critical load (F_{cr}) is determined by the flexural rigidity (D). When the robot is bent, the effective stiffness k_{TC} will increase while the effective stiffness k_{AC} will decrease when the central angle of the continuum robot is increasing, respectively. Effective stiffness modelling and flexural rigidity (D) calculation are part of future work.

VI. CONCLUSION

In this paper, a novel continuum robot named *OctRobot-I* is presented. By designing and applying support spine and layer jamming sheaths, the robot has stiffness variation capability in both transverse and axial directions. A new jamming sheath weaving method using a nylon line and adjacent layers to restrict jamming flaps is proposed, and its length changing ability is evaluated. Four deflection cases of the robot are analysed. Based on the Euler-Bernoulli beam theory and Maxwell-Mohr method, the robot's effective stiffnesses in four cases are defined and derived.

Experiments are conducted with two types of layer jamming sheaths (overlap numbers $n = 3, 5$) and four different vacuum pressures (0kPa, 25kPa, 50kPa, 75kPa) at three different bending angles (0°, 90°, 180°). The results show that when the robot is fitted with the jamming sheath of $n = 3$, the stiffness ranges (ratios) are 36.4 to 241.7N/m (6.6) and 92.9 to 19.3×10^3 N/m (207.8) in the transverse and axial directions, respectively. When fitted with the jamming sheath of $n = 5$, the stiffness ranges (ratios) are 65.7 to 398.3N/m (6.1) and 106.7 to 20.8×10^3 N/m (194.9) in the transverse and axial directions, respectively. In addition, actuating and gripping experiments demonstrated the control and payload of the robot.

Future work includes further improvement of the effectiveness of the stiffness model for numerical analysis of the stiffness variation capability, workspace analysis, real-time position and stiffness control.

REFERENCES

[1] S. Kolachalama and S. Lakshmanan, "Continuum robots for manipulation applications: A survey," *J. Robot.*, vol. 2020, pp. 1–19, Jul. 2020.

[2] S. Li and G. Hao, "Current trends and prospects in compliant continuum robots: A survey," *Actuators*, vol. 10, no. 7, p. 145, Jun. 2021.

[3] J. Burgner-Kahrs, D. C. Rucker, and H. Choset, "Continuum robots for medical applications: A survey," *IEEE Trans. Robot.*, vol. 31, no. 6, pp. 1261–1280, Dec. 2015.

[4] P. E. Dupont, B. J. Nelson, M. Goldfarb, B. Hannaford, A. Menciassi, M. K. O'Malley, N. Simaan, P. Valdastri, and G.-Z. Yang, "A decade retrospective of medical robotics research from 2010 to 2020," *Sci. Robot.*, vol. 6, no. 60, Nov. 2021, Art. no. eabi8017.

[5] M. Wang, "Design, modelling and validation of a novel extra slender continuum robot for in-situ inspection and repair in aeroengine," *Robot. Comput.-Integr. Manuf.*, vol. 67, pp. 1–11, Feb. 2021.

[6] J. Yan, P. Shi, Z. Xu, and J. Zhao, "A wide-range stiffness-tunable soft actuator inspired by deep-sea glass sponges," *Soft Robot.*, vol. 9, no. 3, pp. 625–637, Jun. 2022.

[7] M. Manti, V. Cacucciolo, and M. Cianchetti, "Stiffening in soft robotics: A review of the state of the art," *IEEE Robot. Automat. Mag.*, vol. 23, no. 3, pp. 93–106, Sep. 2016.

[8] L. Blanc, A. Delchambre, and P. Lambert, "Flexible medical devices: Review of controllable stiffness solutions," *Actuators*, vol. 6, no. 3, pp. 1–31, Jul. 2017.

[9] Y. Yang, Y. Li, and Y. Chen, "Principles and methods for stiffness modulation in soft robot design and development," *Bio-Des. Manuf.*, vol. 1, no. 1, pp. 14–25, Mar. 2018.

[10] X. Gao, X. Li, C. Zhao, L. Hao, and C. Xiang, "Variable stiffness structural design of a dual-segment continuum with independent stiffness and angular position," *Robot. Comput.-Integr. Manuf.*, vol. 67, Feb. 2021, Art. no. 102000.

[11] M. Guan, Y. Yan, and Y. Wang, "A bio-inspired variable-stiffness method based on antagonism," in *Proc. 4th Int. Conf. Robot., Control Autom. Eng. (RCAE)*, Nov. 2021, pp. 372–375.

[12] Y. Kim, S. S. Cheng, and J. P. Desai, "Active stiffness tuning of a spring-based continuum robot for MRI-guided neurosurgery," *IEEE Trans. Robot.*, vol. 34, no. 1, pp. 18–28, Feb. 2018.

[13] Z. Xing, F. Wang, Y. Ji, D. McCoul, X. Wang, and J. Zhao, "A structure for fast stiffness-variation and omnidirectional-steering continuum manipulator," *IEEE Robot. Autom. Lett.*, vol. 6, no. 2, pp. 755–762, Apr. 2021.

[14] H. Wang, Z. Chen, and S. Zuo, "Flexible manipulator with low-melting-point alloy actuation and variable stiffness," *Soft Robot.*, vol. 9, no. 3, pp. 577–590, Jun. 2022.

[15] L. Yin, S. Wang, and S. Zuo, "Water-jet outer sheath with braided shape memory polymer tubes for upper gastrointestinal tract screening," *Int. J. Med. Robot. Comput. Assist. Surg.*, vol. 14, no. 6, Dec. 2018, Art. no. e1944.

[16] S. Kitano, T. Komatsuzaki, I. Suzuki, M. Nogawa, H. Naito, and S. Tanaka, "Development of a rigidity tunable flexible joint using magneto-rheological compounds—Toward a multijoint manipulator for laparoscopic surgery," *Frontiers Robot. AI*, vol. 7, pp. 1–8, Apr. 2020.

[17] W. R. Wockenfus, V. Brandt, L. Weisheit, and W.-G. Drossel, "Design, modeling and validation of a tendon-driven soft continuum robot for planar motion based on variable stiffness structures," *IEEE Robot. Autom. Lett.*, vol. 7, no. 2, pp. 3985–3991, Apr. 2022.

[18] S. Jadhav, M. R. A. Majit, B. Shih, J. P. Schulze, and M. T. Tolley, "Variable stiffness devices using fiber jamming for application in soft robotics and wearable haptics," *Soft Robot.*, vol. 9, no. 1, pp. 173–186, Feb. 2022.

[19] A. B. Clark and N. Rojas, "Assessing the performance of variable stiffness continuum structures of large diameter," *IEEE Robot. Autom. Lett.*, vol. 4, no. 3, pp. 2455–2462, Jul. 2019.

[20] D. S. Shah, E. J. Yang, M. C. Yuen, E. C. Huang, and R. Kramer-Bottiglio, "Jamming skins that control system rigidity from the surface," *Adv. Funct. Mater.*, vol. 31, no. 1, Jan. 2021, Art. no. 2006915.

[21] Y. S. Narang, J. J. Vlassak, and R. D. Howe, "Mechanically versatile soft machines through laminar jamming," *Adv. Funct. Mater.*, vol. 28, no. 17, pp. 1–9, Apr. 2018.

[22] Y.-J. Kim, S. Cheng, S. Kim, and K. Iagnemma, "A novel layer jamming mechanism with tunable stiffness capability for minimally invasive surgery," *IEEE Trans. Robot.*, vol. 29, no. 4, pp. 1031–1042, Aug. 2013.

[23] J. L. C. Santiago, I. S. Godage, P. Gonthina, and I. D. Walker, "Soft robots and kangaroo tails: Modulating compliance in continuum structures through mechanical layer jamming," *Soft Robot.*, vol. 3, no. 2, pp. 54–63, Jun. 2016.

[24] E. Amanov, T.-D. Nguyen, S. Markmann, and F. J. I. Burgner-Kahrs, "Toward a flexible variable stiffness endoport for single-site partial nephrectomy," *Ann. Biomed. Eng.*, vol. 46, pp. 1498–1510, May 2018.

[25] A. B. Clark and N. Rojas, "Stiffness-tuneable limb segment with flexible spine for malleable robots," in *Proc. Int. Conf. Robot. Autom. (ICRA)*, May 2019, pp. 3969–3975.

[26] A. B. Clark and N. Rojas, "Malleable robots: Reconfigurable robotic arms with continuum links of variable stiffness," *IEEE Trans. Robot.*, vol. 38, no. 6, pp. 3832–3849, Dec. 2022.

[27] Z. Liu, L. Xu, X. Liang, and J. Liu, "Stiffness-tuneable segment for continuum soft robots with vertebrae," *Machines*, vol. 10, no. 7, p. 581, Jul. 2022.

[28] M. Shen, A. B. Clark, and N. Rojas, "A scalable variable stiffness revolute joint based on layer jamming for robotic exoskeletons," in *Proc. Annu. Conf. Towards Auto. Robotic Syst.* Cham, Switzerland: Springer, 2020, pp. 3–14.

[29] M. Langer, E. Amanov, and J. Burgner-Kahrs, "Stiffening sheaths for continuum robots," *Soft Robot.*, vol. 5, no. 3, pp. 291–303, Jun. 2018.

[30] K. Oliver-Butler, J. Till, and C. Rucker, "Continuum robot stiffness under external loads and prescribed tendon displacements," *IEEE Trans. Robot.*, vol. 35, no. 2, pp. 403–419, Apr. 2019.

Y. Fan et al.: Novel Continuum Robot With Stiffness Variation Capability Using Layer Jamming: Design, Modeling, and Validation

IEEE *Access*

[31] M. M. Dalvand, S. Nahavandi, and R. D. Howe, "An analytical loading model for n-tendon continuum robots," *IEEE Trans. Robot.*, vol. 34, no. 5, pp. 1215–1225, Apr. 2018.

[32] C. M. Wang, J. N. Reddy, and K. H. Lee, "Buckling of columns," in *Shear Deformable Beams and Plates*, 1st ed. Amsterdam, The Netherlands: Elsevier, 2000, pp. 55–75.

[33] D. B. Camarillo, C. F. Milne, C. R. Carlson, M. R. Zinn, and J. K. Salisbury, "Mechanics modeling of tendon-driven continuum manipulators," *IEEE Trans. Robot.*, vol. 24, no. 6, pp. 1262–1273, Dec. 2008.

[34] I. A. Karnovsky and O. Lebed, *Advanced Methods of Structural Analysis*. Boston, MA, USA: Springer, 2010.

DIKAI LIU (Senior Member, IEEE) received the Ph.D. degree in dynamics and control from the Wuhan University of Technology, Wuhan, China, in 1997.

He is currently a Professor with the Robotics Institute, University of Technology Sydney, Sydney, Australia. His main research interests include robotics, including robot perception, planning and control of mobile manipulators operating in complex environments, human–robot collaboration, multi-robot coordination, and bioinspired robotics.

YEMAN FAN (Student Member, IEEE) received the B.E. degree in machine designing, manufacturing and automation and the M.E. degree in agricultural electrification and automation from Northwest A&F University, Yangling, China, in 2016 and 2019, respectively. He is currently pursuing the Ph.D. degree with the Robotics Institute, University of Technology Sydney, Sydney, NSW, Australia.

His research interests include continuum robots and manipulators, robot control systems, and jamming technology for robot.

LIN YE received the B.E. degree from Harbin Engineering University, in 1982, and the M.E. and Ph.D. degrees from Beihang University, in 1984 and 1987, respectively.

He is a Professor with the School of Aerospace, Mechanical and Mechatronic Engineering, The University of Sydney, Australia. His research interests include composites science and technology, smart materials and structures, nano-materials and nano-composites, and structural integrity and durability.

• • •